

Strain Analysis in GaN Layer on Si (100) Substrate and Impact of GaN Porosity for Strain Reduction

Noratiqah Yusop,¹ Siti Nurul Waheeda,¹ Norzaini Zainal,^{1*} Ross E. L. Powell² and Anthony J. Kent²

¹Institute of Nano Optoelectronics Research and Technology (INOR),
Universiti Sains Malaysia, 11800 USM, Pulau Pinang, Malaysia

²School of Physics and Astronomy, University of Nottingham,
Nottingham NG7 2RD, United Kingdom

*Corresponding author: norzaini@usm.my

Published online: 21 April 2025

To cite this article: Yusop, N., Waheeda, S. N., Zainal, N., Powell, R. E. L. & Kent, A. J. (2025). Strain analysis in GaN layer on Si (100) substrate and impact of GaN porosity for strain reduction. *J. Phys. Sci.*, 36(1), 1–16. <https://doi.org/10.21315/jps2025.36.1.1>

To link this article: <https://doi.org/10.21315/jps2025.36.1.1>

ABSTRACT: *Strain effects in gallium nitride (GaN) layer grown on silicon (Si) (100) substrate are investigated. Results from Raman spectroscopy measurements suggested that the stress level in the GaN layer is around -0.48 GPa that is higher than several reported values. Moreover, the coherency of the GaN layer with respect to the Si substrate was confirmed by X-ray diffraction (XRD)-reciprocal space mapping XRD-RSM measurement. As derived from XRD ω -rocking curve, the strain was around 0.0216 and -0.0241 along c -axis and a -axis, respectively. Meanwhile, results from temperature-dependent photoluminescence (PL) measurements indicated that the strain in the layer can be influenced by the binding energy of donors. In the effort to achieve strain reduction, few micrometres of the GaN layer were fabricated into porous structure. In particular, a sample was prepared without annealing treatment, and another was subjected to annealing treatment at 800°C prior to etching (pre-annealing). It was found that the strain was reduced with the porous structure, especially by the pre-annealing treatment.*

Keywords: strain, GaN, porous, etching, pre-annealing

1. INTRODUCTION

Remarkable progress of fabrication technology nowadays enables gallium nitride (GaN) semiconductor compounds to be on the top priority in material selections for modern devices.^{1,2} In the pursuit of reducing the fabrication cost of GaN-

based devices, using silicon (Si) as the substrate for the devices' heterostructure has been widely accepted as one of the preferred methods.³ Nonetheless, such heteroepitaxial growth is not only introducing a high dislocation density and cracks to the GaN layers, but also adding strain due to lattice mismatch and thermal expansion coefficient between the films and the substrate, which can affect the overall quality of GaN layer. Several approaches have been demonstrated in the effort to reduce strain in the GaN layer-grown Si substrate for many years. Of common technique to achieve this target is by inserting aluminium nitride (AlN) as an intermediate layer, of which a thin layer of AlN is grown as a buffer layer in the growth of GaN on Si substrate. The AlN layer is beneficial to mitigate the impact of strain and to prevent GaN melt-back etching which can degrade the subsequent GaN growth.⁴ However, the strain continues to rise with increasing thickness. In addition, other studies have reported on adopting two-step growth of AlN.^{5,6} Specifically, by alternately applying low-temperature and high-temperature growth. This method results in compressive strain in the overgrown GaN layer by compensating the existing tensile strain. However, from the epitaxial point of view, this method requires precise control of the growth temperature in a short period of time. Moreover, achieving optimum growth conditions of AlN is a complicated task since III/IV ratio, pressure, as well as temperature can significantly influence the final growth.^{7,8} Meanwhile, epitaxial lift-off method has been demonstrated to reduce the strain in GaN layers grown on bulk GaN and SiC substrates.^{9,10} Nevertheless, apart from involving intricate steps and utilisation of expensive instruments, the use of the laser during the experiment can cause damage to the GaN layers.^{11,12} The result could be worse for GaN layers on Si substrate. Alternatively, porous GaN is proposed as a promising approach to achieve strain reduction in the GaN layers and GaN-based heterostructures.¹³⁻¹⁵ This approach has not been widely applied for GaN layers on Si substrate by far, especially through straightforward manners. In our previous study, we proposed a new alternative method to reduce the strain in molecular beam epitaxy (MBE)-grown GaN layer on Si substrate.¹⁶ Specifically, by annealing the layer before the fabrication of a few nanometres of GaN layer into a porous structure through electrochemical etching. Here, we intend to expand the scope of the previous study by closely investigating the strain in the GaN layers grown on Si and the impact of the GaN porosity for the strain reduction.

Studies on porous GaN have been widely explored due to its intriguing properties, which are beneficial for environmental applications, e.g., high humidity and high temperatures. The porous GaN structure was utilised as a template for zinc oxide (ZnO) deposition, aimed at improving humidity sensor applications due to its high chemical stability and high-surface-to-volume ratio, i.e., larger surface interaction with the environment, compared to their bulk counterpart.¹⁷ These

features enhance its sensitivity to humidity and provide more effective electron transfer, improving the overall sensing performance of the devices. Moreover, a recent study has demonstrated a combination of porous GaN/Nickel-cobalt oxides (NCO) (binary transition metal oxides) is capable of powering LED up to five units and can provide a maximum power density of 44.0 mWcm^{-2} , due to the enhanced conductivity and short conductive channels.¹⁸ Meanwhile, a published work found that porous GaN exhibited better electronic and optical properties compared to non-porous GaN, making it suitable for gas sensing and UV photodetectors.^{19,20} Therefore, the strain reduction in porous GaN as demonstrated here can be useful for achieving GaN-based devices with improved electronic and optical properties. Hence, the present study focuses on strain analysis for a GaN layer on Si substrate, along with discussions on the material properties of porous GaN/GaN layer (porous GaN sample), specifically addressing the strains involved. Based on our previous work, the etching effect becomes more significant for the sample annealed prior to the etching (pre-annealing).¹⁶ Therefore, the impact of pre-annealing on releasing the strain in the porous GaN/GaN layer is also investigated here.

2. EXPERIMENTAL PROCEDURES

Here, an undoped GaN layer was epitaxially grown on a 3-inch commercial n-type (100)-oriented cubic Si substrate in Veeco GEN-II RF-plasma assisted MBE reactor. The surface of the Si substrate was cleaned first by exposing the Ga flux at a temperature of 850°C to remove SiO_2 particles from the surface. In order to avoid melt-back etching due to the interaction between Ga atoms and Si at high temperatures, a thin AlN layer with the thickness of around 200 nm–300 nm was grown as a buffer layer at 840°C . This was followed by growing a 0.2 μm thick GaN layer at the same temperature.

The stress level in the GaN layer was investigated by Bruker Dimension Edge Model-Raman spectroscopy. The Raman measurement was carried out under $z(y, \text{unpolarised})\bar{z}$ scattering configuration. Such configuration allows the signals for $E_2(\text{high})$ and $A_1(\text{LO})$ modes of GaN which can provide an insight into the strain state and residual carrier concentration due to dislocations or defects, respectively.²¹ The shift in the $E_2(\text{high})$ peak position of the GaN layer with respect to a bulk GaN (unstrained) was taken into account to determine the stress level in the layer.²¹ Through X-ray diffraction (XRD)-reciprocal space mapping (XRD-RSM) measurement, the coherency of the GaN layer to the AlN buffer layer was confirmed. Next, XRD ω -rocking curve (XRC) measurements in (002) symmetric and (102) asymmetric reflections were performed using XRD (Bruker-D8) to evaluate the crystalline properties and to estimate the amount of strain in the

GaN layer. The dependence of the GaN peaks related to emission energy on temperature was determined from temperature-dependent photoluminescence (PL) measurements using a frequency-tripled titanium (Ti): Sapphire laser with a power of 5 mW at 266 nm (Spectra-Physics Tsunami). Such dependence can provide insights on the effect of strain in the GaN layer. The binding energy of donors was also estimated from the temperature dependence of the energy of the emission peak due to donor-acceptor (DAP) and free electron-to-acceptor level (eA) recombination.

Subsequently, a porous GaN/GaN layer (see Figure 1) was fabricated through electrochemical etching using 5% sodium hydroxide (NaOH) solution as the electrolyte within 15 min. The etching process was assisted by UV illumination. A porous GaN/GaN layer with pre-annealing at 800°C was also fabricated to observe the impact of the pre-annealing in releasing the strain in the GaN layer further. The annealing temperature of 800°C was selected based on our previous optimisation work.¹⁶ The characteristics of the porous GaN were observed under a scanning electron microscope (SEM) (FEI Nova NanoSEM 450). The strain properties in the porous GaN samples were also investigated.

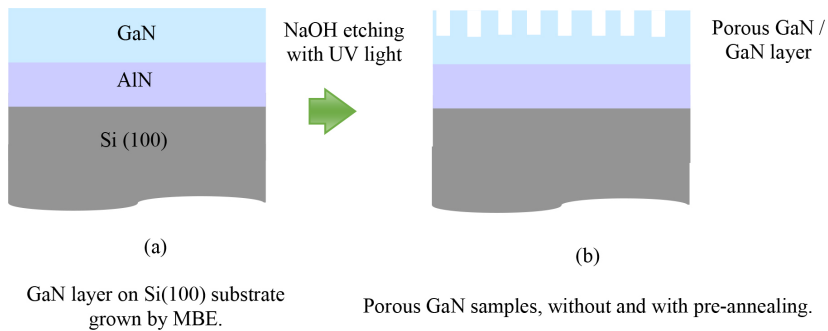


Figure 1: Growth of a GaN layer on Si(100) substrate with AlN buffer layer and preparation of porous GaN samples.

3. RESULTS AND DISCUSSIONS

Figure 2 shows Raman spectrum of the GaN layer grown on Si (100) substrate. The peak at $\sim 565 \text{ cm}^{-1}$ can be assigned to GaN E_2 (high) mode and $\sim 732 \text{ cm}^{-1}$ to GaN $A_1(\text{LO})$ mode. The $E_2(\text{high})$ peak position is commonly regarded as sensitive to biaxial stress with 1 GPa causing a shift of 4.2 cm^{-1} from an unstrained sample.²² By considering a reported unstrained bulk layer with the E_2 (high) peak of 567 cm^{-1} , the E_2 (high) peak of the GaN layer in the present study shifts towards lower energy sides.²³ The estimation gives the biaxial stress in the GaN layer to be

around -0.48 GPa. The value is about 10 times higher than a reported GaN layer on a 6H-SiC substrate and about 3 times higher than a reported GaN layer on Si (111) substrate.^{24,25} The negative sign shows the GaN is under tensile stress.²⁴ The $E_2(\text{high})$ peak at $\sim 655\text{ cm}^{-1}$ is due to the AlN buffer layer. Moreover, the intensity of the $A_1(\text{LO})$ peak is too weak, suggesting the GaN layer has a high residual carrier density.²⁶

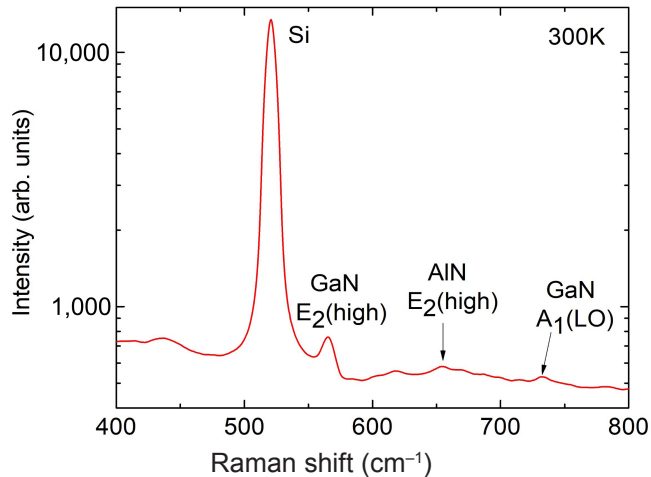


Figure 2: Raman spectrum of a GaN layer grown on Si (100) substrate.

Given the fact that the crystalline properties of the GaN layer can be correlated to its strain behaviours, therefore, XRD measurement in 2θ scans was conducted and the results are shown in Figure 3. It is evident that the layer was preferentially grown in the $[0002]$ direction. The peak of the AlN buffer layer also appears in the data. It is interesting to note that the XRD peak of cubic is invisible although the GaN layer was on the cubic substrate. In general, the initiation of cubic growth without proper growth conditions (e.g., temperature) is unlikely since cubic GaN is thermodynamically unstable.^{27,28} Additionally, cubic growth is hard to achieve due to the large difference in the lattice constant between GaN and Si substrate.²⁹ Therefore, hexagonal GaN, a thermodynamically stable structure was predominantly grown and the impact of the cubic GaN phase materials on the strain can be negligible.

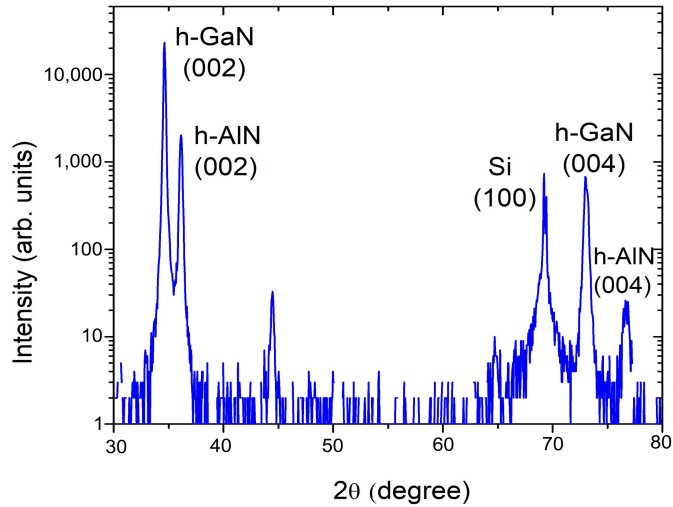


Figure 3: 2 θ -XRD data of a GaN layer grown on Si (100) substrate.

Figure 4(a) shows the results of XRD-RSM measurement in (002) reflection for the GaN layer grown on Si (100). From the results it can be seen that the peak of GaN layer aligns with the peak of the AlN buffer layer. This reveals that the GaN layer is in a coherent strained condition. As shown in Figure 4(b), the broadening of the diffraction peak in q_x direction from the asymmetric (-105) reflection is evident. The peak broadening can be attributed to in the strain level of the GaN layer.³⁰

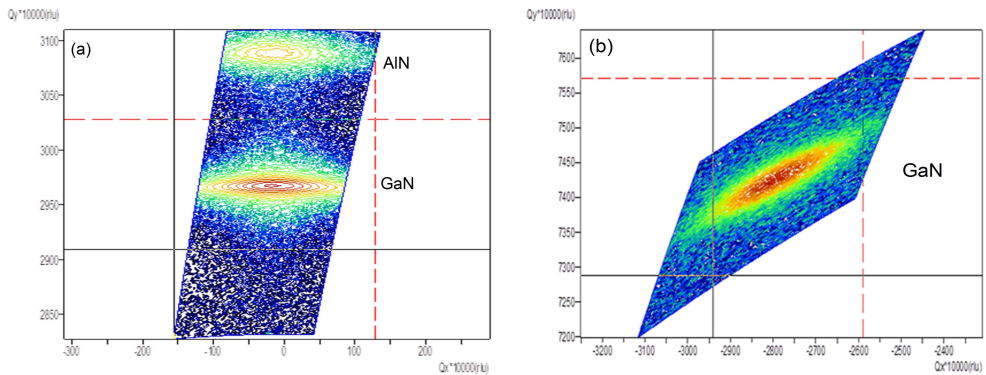


Figure 4: (Color online) XRD-RSM of (a) symmetric (002) and (b) asymmetric (-105) reflections for a GaN layer grown on Si (100) substrate.

The crystalline quality of the GaN layer was assessed by XRC measurement in (002) and (102) reflections. From the results, the vertical strain, ε_c and horizontal strain, ε_a in the GaN layer can be estimated using the Equation 1.³¹

$$\varepsilon_c = (c - c_o) / c_o \quad , \quad \varepsilon_a = (a - a_o) / a_o \quad (1)$$

Where c_o and a_o are the lattice constant of a bulk GaN with value of 5.185 Å and 3.189 Å, respectively.³² From the strain value obtained through Equation 1, it can be used to estimate the biaxial stress, σ in the GaN layer using Equation 2.

$$\varepsilon_c = -E^{-1}\sigma_c 2\nu \quad , \quad \varepsilon_a = E^{-1}\sigma_a (1-\nu) \quad (2)$$

Where ν represents the Poisson ratio, while the E is the Young Modulus with value of 196 GPa.³² The lattice constant of a and c can be calculated using Equation 3 and Equation 4 as below.³³ The lattice constants a and c should be determined prior to the estimation for the strain and stress.

$$n\lambda = 2d_{hkl} \sin \theta \quad (3)$$

$$1/d_{hkl}^2 = 4/3 ((h^2 + k^2 + hk)/a^2) + (l^2 + c^2) \quad (4)$$

Where, λ is the wavelength of the X-ray, θ_{hkl} is the measured Bragg angle and d_{hkl} is the lattice spacing of the crystal plane.

Figure 5 shows the XRC of the GaN layer in (002) and (102) reflections. Full width at half maximum of the XRC (FWHMs-XRC) is 1.340° or 4,824 arcsec in (002) reflection and 0.024° or 86.4 in arcsec (102) reflection. From the calculations, the lattice constant, a and c of the GaN layer is 3.112 Å and 5.297 Å, respectively. Hence, ε_c and ε_a of the GaN layer is 0.0261 and -0.0241, respectively.

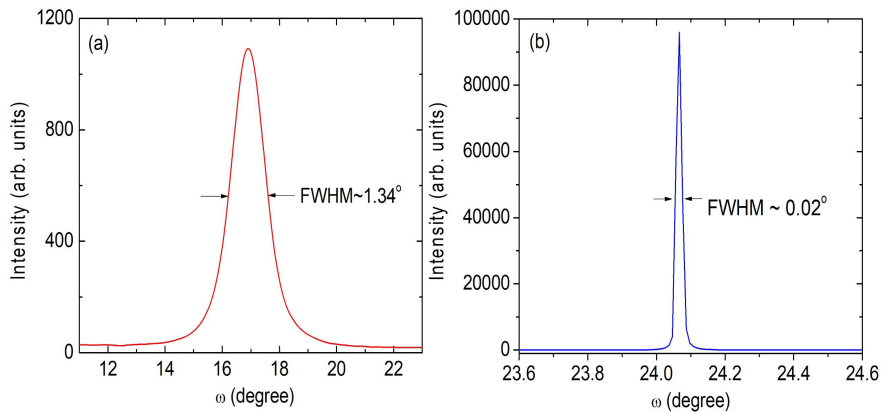


Figure 5: XRC in (a) (002) symmetric reflection, and (b) (102) asymmetric reflection of a GaN layer grown on Si (100) substrate.

As revealed from the Raman measurement (Figure 2), it is found that the GaN layer grown on Si substrate (before annealing and etching) is under tensile strain with the estimated biaxial stress of 0.48 GPa. Meanwhile, as measured by XRD, in-plane lattice constant, a of the GaN layer is around 3.112 Å, which is smaller than the in-plane lattice constant, a of a bulk GaN. Assuming biaxial stress, the decrease in the lattice constant of the GaN layer is leading to higher compressive strain. In general, GaN layer grown on Si substrate suffers from high tensile strain due to a larger lattice constant of Si with respect to the GaN layer. The contradicting result obtained from both Raman and XRD measurements indicates that several mechanisms are acting in different directions towards determining the final strain level of the GaN layer.

Next, it is interesting to observe how PL emissions in the GaN layer can be influenced by strain. Figure 6(a) shows PL spectra of the GaN grown on Si (100) substrate measured at 4 K. A sharp and intense peak at ~3.5 eV can be attributed to near band-edge emission (NBE) of GaN. Additionally, a weak shoulder peak as seen around 3.2 eV is related to DAP transitions. The yellow luminescence bands are reflected by a broad peak centred at ~2.5 eV which is typically due to various defects, e.g., Ga and N vacancies.^{34,35}

Figure 6(b) shows the dependence of PL emission peak energy against temperature. In the present study, Gaussian fitting was adopted to distinguish the overlapping peaks of DAP and eA transitions. From the results, it can be seen that the NBE peak emission shifts towards lower energies as the temperature increases. This is commonly observed due to band gap shrinking at elevated temperatures, as explained by Varshni's equation.

$$E(T) = E(0) - \alpha T^2 / (T + \theta) \quad (5)$$

Where $E(T)$ is the transition energy at temperature, T and $E(0)$ is band gap energy at 0 K.³⁶ Moreover, α and θ refer to the thermal coefficient and Debye temperature of 600 K, respectively. The measured data shows the best fit with fitting parameters, where $\alpha = 4.78 \times 10^{-4}$ eV K⁻¹, slightly below the reported value of 5×10^{-4} eV K⁻¹.³⁷

It is obvious that the DAP transitions became more important than the eA transitions at low temperatures. In general, increased temperatures promote the ionisation of the electrons at donor levels, thereby allowing their transition to the conduction band. This, in turn, results in free electrons which recombine with holes at the valence band, leading to eA transitions. Correspondingly, the DAP transitions turn into eA transitions with increasing temperatures, causing the peak emission to shift towards blue spectrum. The emission energy of the transitions

with temperature is given by,

$$E(eA) = E_g(T) - E_A + 1/2k_B T \quad (6)$$

Where, $1/2k_B T$ is the mean energy of free electrons in the conduction band. According on Equation 6, the binding energy of the acceptor (E_A) is around 130 meV. Meanwhile, the energy separation between the DAP and eA transitions is nearly 44 meV. This is corresponded to the binding energy of the donors (E_D). This value is above the reported binding energy of deep donors, while is significantly higher than that of Si and O donors.^{38–40} An earlier work in reported that the donors binding energy can be increased by stress.⁴¹ This could be the case in the present study. It is worth noting that the biaxial stress in the GaN film is estimated at around -0.48 GPa (see Figure 2), which is higher than some published works.^{24,25}

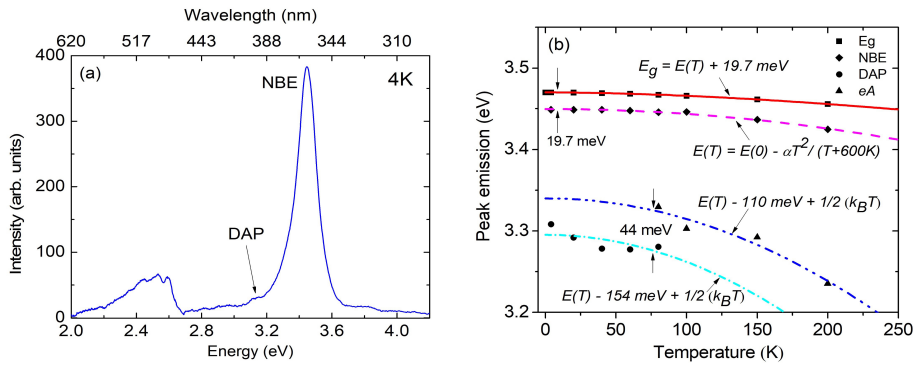


Figure 6: (a) PL spectrum of a GaN layer grown on Si (100) substrate and (b) dependence of PL peak emission energy on temperature.

Subsequently, the results for the samples of porous GaN/GaN layer (porous GaN samples) are presented. In particular, one was fabricated without annealing and another with pre-annealing at 800°C . Figure 7 shows the surface morphology of the porous GaN/GaN layer samples, including the non-porous sample (the GaN layer as described in the previous sections) and the non-porous sample annealed at 800°C for comparison. From atomic force microscopy (AFM) measurements (data is not shown here), root mean square (RMS) surface roughness for the annealed non-porous sample is slightly lower than that of the non-annealed non-porous sample. Meanwhile, the etching effect is more noticeable for the pre-annealed porous sample compared to the one without annealing, where dense porosity is observed. This can be related to the impact of the pre-annealing. Specifically, the re-crystallisation of disordered atomic lattice structures occurred during

annealing. This allows more holes to accumulate on the surface through the photo-generated carriers with the assistance from the UV illumination.⁴² It has been widely observed that higher number of holes on the surface enhances the etching activity.⁴³

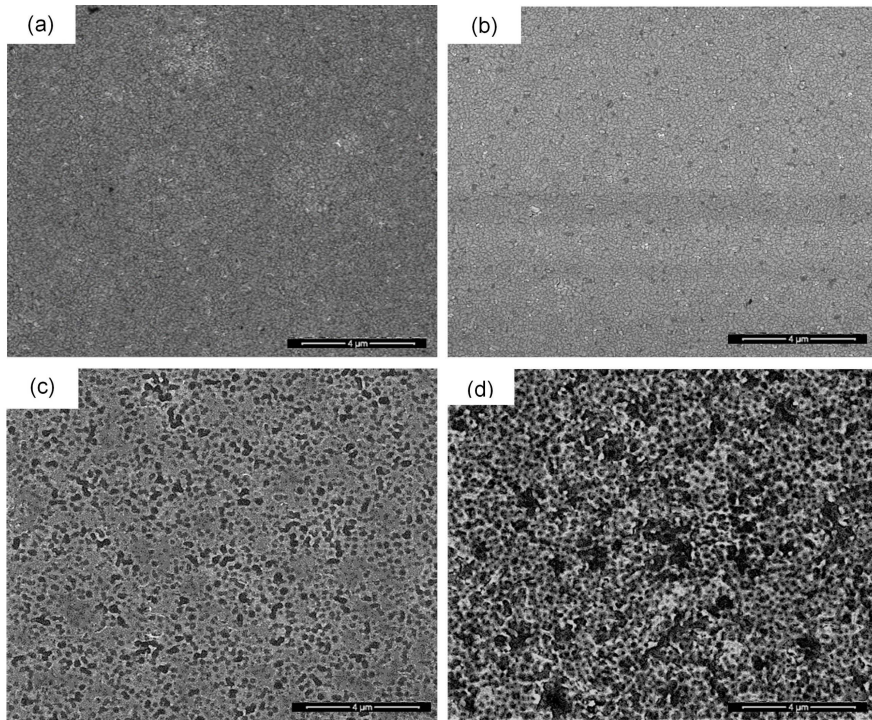


Figure 7: Top-view SEM images of (a) non-porous GaN, (b) non-porous GaN after annealed at 800°C, (c) porous GaN without annealing and (d) porous GaN with 800°C pre-annealing.

Moreover, the annealing treatment reduces threading dislocations which usually trap the photo-generated carriers on the surface.¹⁴ The FWHMs-XRC for the pre-annealed GaN layer on Si (before etching) is 1.168° or 4,204.8 arcsec in (002) reflection and 0.023° or 82.8 arcsec in (102) reflection. The (002) FWHM for the sample is lower than the non-annealed GaN layer (see Figure 5), while there is no significant change for (102) FWHM, see Table 1.

Strictly speaking, it is hard to obtain XRC for porous samples, especially for the XRC in (102) reflection. Here, the FWHMs-XRC in (002) reflection for the non-annealed porous GaN shows a higher value of 5,328 arcsec than the pre-annealing porous GaN with 5,004 arcsec, implying that the crystal quality of the porous

GaN can be improved under thermal treatment. However, the FWHM values of the porous GaN are higher than the non-porous GaN. This is associated with the reduction of the X-ray coherence length when the X-rays were incident on the surface with open spaces, i.e., pores in our case. As a result, this leads to the noticeable broadening of the XRC. Moreover, non-stoichiometry of Ga or N surface resulted from the etching can increase the FWHMs for the porous GaN samples.⁴⁴ Nonetheless, the FWHMs for the porous GaN samples are comparable to the reported porous GaN on sapphire substrate.⁴⁵ By annealing the sample prior to the etching (pre-annealing), the FWHMs can be reduced. Table 1 summarises the results from the XRC measurements.

Table 1: FWHMs of XRC in (002) and (102) reflections for non-porous and porous GaN samples.

Sample	(002) FWHM-XRC (arcsec)	(102) FWHM-XRC (arcsec)
Non-porous GaN	4,824.0	86.4
Annealed non-porous GaN	4,204.8	82.8
Porous GaN without annealing	5,328.0	–
Porous GaN with pre-annealing	5,004.0	–

Figure 8(a) shows the in-plane lattice constant, a and the out-plane lattice constant, c for the porous GaN samples, as estimated through the XRC measurements. Also included is the result for the non-porous GaN sample that is obtained from Figure 5. Apparently, the lattice constants of the porous samples, especially for the sample with pre-annealing are closer to the bulk GaN (shown by dashed lines) compared to the non-porous sample. Meanwhile, Figure 8(b) shows the calculated strain in a -axis, ε_a and c -axis, ε_c , respectively. In line with Figure 8(a), the strain in both directions can be reduced with the porous layer. This indicates that the porous layer is beneficial to release parts of strain inside the GaN layer. The result is more significant for the porous GaN with pre-annealing, of which the process promotes considerable porous formation (Figure 7). This implies that the porous GaN/GaN layer can be a useful template for the growth of GaN-based heterostructure. Specifically, the porous GaN can act as a strain-relieved layer while prohibiting the threading dislocations propagation into the next layers.^{13–15,46}

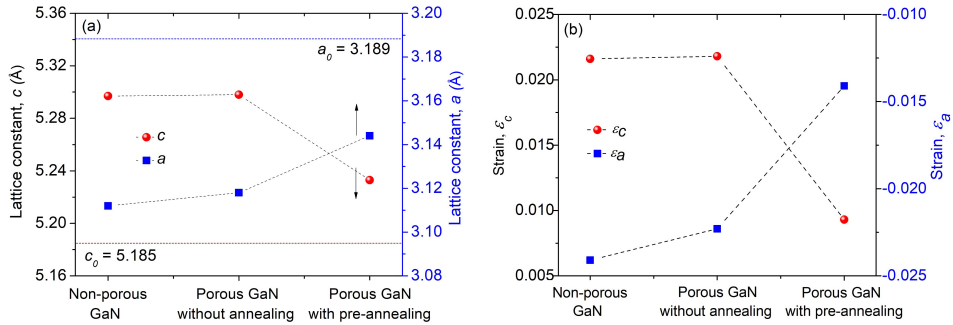


Figure 8: (a) Lattice constants and (b) calculated strain for non-porous GaN and porous GaN, without annealing and with pre-annealing.

Table 2 shows the NBE peak of the porous GaN samples as measured at 300 K. The NBE peak of the porous sample shifts towards shorter wavelengths in comparison to the non-porous sample. The result is more evident for the porous GaN with pre-annealing. With respect to the non-porous sample, the NBE peak for the porous GaN with pre-annealing shows 176 meV blue-shift. An increase in the energy gap is related to increase in compressive strain. Correspondingly, some amounts of the tensile strain (Figure 2) were released through the etching process.

Table 2: Near band-edge emission PL peak energy for non-porous and estimated tensile stress reduction with respect to the non-porous GaN.

Sample	NBE peak energy (eV)	Tensile stress reduction (GPa)
Non-porous GaN	3.399	–
Porous GaN without annealing	3.457	2.75
Porous GaN with pre-annealing	3.575	8.34

4. CONCLUSION

The present study found that the GaN layer grown on Si (100) substrate consists of a high tensile stress of 0.48 GPa. Despite the FWHM-XRC for the GaN layer in (002) reflection is significantly higher than the reported GaN layers grown on SiC and sapphire, the (102) FWHM-XRC of the layer is about 3–5 times lower.²⁴ This shows that the GaN layer was grown in a good crystalline structure although using its large lattice-mismatched Si (100) substrate. The strain can be released by fabricating a few micrometres of the GaN layer from the surface into the porous structure. Further strain reduction was achieved by subjecting the sample to an

annealing treatment at 800°C before the etching process (pre-annealing). The proposed porous GaN/GaN layer has the potential to enable the growth of thicker heterostructures since the porous can act as a strain-relieved layer while being able to ‘sink’ the threading dislocations in the overgrown heterostructures.

5. ACKNOWLEDGEMENTS

The authors would like to thank the Ministry of Higher Education Malaysia for funding this project via the Higher Education Centre of Excellence (HiCoE), Institute of Nano Optoelectronics Research and Technology (INOR) under account number A305-KR-AKH002-0000000431-K134. We also thank Mr. Jingyi Chen from Panalytical (China) for his assistance with the XRD-RSM measurements.

6. REFERENCES

1. Nik Sin, N. F., Ibrahim, K. & Zainal, N. (2019). Growth of bulk gallium nitride single crystal by sodium flux method: A brief review. *J. Phys. Sci.*, 30(2), 189–208. <https://doi.org/10.21315/jps2019.30.2.11>
2. Alias, E. A. et al. (2015). Thermal annealing effects on the properties of MBE-GaN p-n junction. *J. Phys. Sci.*, 26(1), 35–42.
3. Alias, E. A. et al. (2021). Luminescence and crystalline properties of InGaN-based LED on Si substrate with AlN/GaN superlattice structure. *J. Phys. Sci.*, 32(3), 1–11. <https://doi.org/10.21315/jps2021.32.3.1>
4. Luo, W. et al. (2008). Influence of AlN buffer layer thickness on the properties of GaN epilayer on Si (111) by MOCVD. *Microelectron. J.*, 39(12), 1710–1713. <https://doi.org/10.1016/j.mejo.2008.01.042>
5. Deura, M. et al. (2023). Effect of layer structure of AlN interlayer on the strain in GaN layers during metal-organic vapor phase epitaxy on Si substrates. *J. Appl. Phys.*, 133(16), 165301. <https://doi.org/10.1063/5.0143985>
6. Lin, P. J. et al. (2017). On the role of AlN insertion layer in stress control of GaN on 150-mm Si (111) substrate. *Crystals*, 7(5), 134. <https://doi.org/10.3390/cryst7050134>
7. Altuntas, I. et al. (2021). Influence of the PALE growth temperature on quality of MOVPE grown AlN/Si (111). *Mater. Sci. Semicond. Process.* 127, 105733. <https://doi.org/https://doi.org/10.1016/j.mssp.2021.105733>
8. Adikimenakis, A. et al. (2009). Effect of AlN interlayers in the structure of GaN-on-Si grown by plasma-assisted MBE. *J. Cryst. Growth*, 311(7), 2010–2015. <https://doi.org/10.1016/j.jcrysgro.2008.10.085>
9. Mu, F. et al. (2017). GaN-Si direct wafer bonding at room temperature for thin GaN device transfer after epitaxial lift off. *Appl. Surf. Sci.*, 416, 1007–1012. <https://doi.org/10.1016/j.apsusc.2017.04.247>

10. Voronenkov, V. (2019). Laser slicing: A thin film lift-off method for GaN-on-GaN technology. *Results Phys.*, 13, 27–30. <https://doi.org/10.1016/j.rinp.2019.102233>
11. Zhang, L. et al. (2017). One-step fabrication of porous GaN crystal membrane and its application in energy storage. *Sci. Reports*, 7, 1–9. <https://doi.org/10.1038/srep44063>
12. Han, Y. et al. (2017). Lattice disorder produced in GaN by He-ion implantation. *Nucl. Instrum. Methods Phys. Res. B*, 406, 543–547. <https://doi.org/10.1016/j.nimb.2016.12.039>
13. Yao, Y. et al. (2023). The development and applications of nanoporous gallium nitride in optoelectronics: a review. *Semicond. Sci. Technol.*, 38(7), 74001. <https://doi.org/10.1088/1361-6641/accd14>
14. Hartono, H. et al. (2007). Reduction of threading dislocation density in GaN grown on strain relaxed nanoporous GaN template. *Appl. Phys. Lett.*, 90(17), 171917. <https://doi.org/10.1063/1.2732826>
15. Ji, Y. et al. (2023). Porous pseudo-substrates for InGaN quantum well growth: Morphology, structure, and strain relaxation. *J. Appl. Phys.*, 134(14), 145102. <https://doi.org/10.1063/5.0165066>
16. Waheeda, S. N., Zainal, N. & Hassan, Z. (2015). Role of pre-annealing treatment in improving the porosity of gallium nitride on cubic silicon (100) substrate. *Mater. Sci. Semicond. Process.*, 30, 330–334. <https://doi.org/10.1016/j.mssp.2014.10.022>
17. Wang, C. et al. (2019). A ZnO/porous GaN heterojunction and its application as a humidity sensor. *Nanoscale Adv.*, 1(3), 1232–1239. <https://doi.org/10.1039/c8na00243f>
18. Lv, S. et al. (2023). Gallium nitride-based electrode for high-temperature supercapacitors. *Adv. Sci.*, 10(15), 1–10. <https://doi.org/10.1002/advs.202300780>
19. Beh, K. P. et al. (2013). Photoelectrochemical fabrication of porous GaN and their applications in ultraviolet and ammonia sensing. *Jap. J. Appl. Phys.*, 52(8S). <https://doi.org/10.7567/JJAP.52.08JK03>
20. Yu, R. et al. (2019). From bulk to porous GaN crystal: Precise structural control and its application in ultraviolet photodetectors. *J. Mater. Chem. C*, 7(45), 14116–14122. <https://doi.org/10.1039/c9tc04820k>
21. Harima, H. (2002). Properties of GaN and related compounds studied by means of Raman scattering. *J. Phys. Condensed Matter*, 14(38). <https://doi.org/10.1088/0953-8984/14/38/201>
22. Kisielowski, C. et al. (1996). Strain-related phenomena in GaN thin films. *Phys. Rev. B - Condensed Matter Mater. Phys.*, 54(24), 17745–17753. <https://doi.org/10.1103/PhysRevB.54.17745>
23. Goñi, A.R. et al. (2001). Effect of pressure on optical phonon modes and transverse effective charges in GaN and AlN. *Phys. Rev. B - Condensed Matter Mater. Phys.*, 64(3), 1–6. <https://doi.org/10.1103/PhysRevB.64.035205>
24. Shao, Y. et al. (2023). Crystallographic orientation and stain in GaN Crystals Grown on 6H-SiC and Sapphire Substrates. *Crystals*, 13(12), 1694. <https://doi.org/10.3390/cryst13121694>

25. Kukushkin, S. A. et al. (2018). Plasma assisted molecular beam epitaxy of thin GaN films on Si (111) and SiC/Si (111) substrates: Effect of SiC and polarity issues. *Thin Solid Films*, 646, 158–162. <https://doi.org/10.1016/j.tsf.2017.11.037>
26. Eric N'Dohi, A. J. et al. (2022). Micro-Raman characterization of homo-epitaxial n doped GaN layers for vertical device applications. *AIP Adv.*, 12(2), 025126. <https://doi.org/10.1063/5.0082860>
27. Laifi, J. C. et al. (2017). Study of cubic GaN clusters in hexagonal GaN layers and their dependence with the growth temperature. *Vacuum*, 138, 8–14. <https://doi.org/10.1016/j.vacuum.2017.01.007>
28. Okura, K. et al. (2019). Growth temperature dependence of cubic GaN step structures and cubic InN dot arrays grown on MgO (001) vicinal substrates. *Jap. J. Appl. Phys.*, 58(SC). <https://doi.org/10.7567/1347-4065/ab106a>
29. Binks, D. J. et al. (2022). Cubic GaN and InGaN/GaN quantum wells. *Appl. Phys. Rev.*, 9(4), 041309. <https://doi.org/10.1063/5.0097558>
30. Li, Z. et al. (2017). Semi-polar (11-22) AlGaIn on overgrown GaN on micro-rod templates: Simultaneous management of crystal quality improvement and cracking issue. *Appl. Phys. Lett.*, 110(8), 082103. <https://doi.org/10.1063/1.4977094>
31. Lagerstedt, O. & Monemar, B. (1979). Variation of lattice parameters in GaN with stoichiometry and doping. *Phys. Rev. B*, 19(6), 3064–3070. <https://doi.org/10.1103/PhysRevB.19.3064>
32. Alaei, H. R. et al. (2010). Thermal stress and strain in a GaN epitaxial layer grown on a sapphire substrate by the MOCVD method. *Chin. J. Phys.*, 48(3), 400–407.
33. Moram, M. A. & Vickers, M. E. (2009). X-ray diffraction of III-nitrides. *Reports Progress Phys.*, 72(3). <https://doi.org/10.1088/0034-4885/72/3/036502>
34. Hellman, E. S. et al. (1996). ScAlMgO₄: An oxide substrate for GaN epitaxy. *MRS Internet J. Nitride Semicond. Res.*, 1,1. <https://doi.org/10.1557/S1092578300001733>
35. Santana, G. et al. (2014). Photoluminescence spectroscopy as a tool for quality control of GaN thin film to be used in solar cell devices. *2014 IEEE 40th Photovoltaic Specialist Conference (PVSC)*, Denver (USA), 2014, pp. 1852–1854, <https://doi.org/10.1109/PVSC.2014.6925284>
36. Xu, S. J. et al. (2001). Defect states in cubic gan epilayer grown on gas by metalorganic vapor phase epitaxy. *Phys. Status Solidi A Appl. Res.*, 188(2), 681–685. [https://doi.org/10.1002/1521-396X\(200112\)188:2<681::AID-PSSA681>3.0.CO;2-7](https://doi.org/10.1002/1521-396X(200112)188:2<681::AID-PSSA681>3.0.CO;2-7)
37. Kim, D. K. & Park, C. B. (2005). Photoluminescence studies of GaN films on Si(111) substrate by using an AlN buffer control. *J. Korean Phys. Soc.*, 47, 1006–1009.
38. Freitas, J. A. et al. (2003). Shallow donors in GaN. *Phys. Status Solidi B Basic Res.*, 240(2), 330–336. <https://doi.org/10.1002/pssb.200303402>
39. Strite, S. & Morkoç, H. (1992). GaN, AlN, and InN: A review. *J. Vac. Sci. Technol. B Microelectron. Nanometer Struct. Process. Meas. Phenom.*, 10(4), 1237–1266. <https://doi.org/10.1116/1.585897>
40. Freitas, J. A. (2020). Pervasive shallow donor impurities in GaN. *ECS J. Solid State Sci. Technol.*, 9(1), 015009. <https://doi.org/10.1149/2.0272001jss>

41. Oyoko, H. O. et al. (2004). Theoretical study of the effect of applied stress on the binding energy of a donor impurity in GaAs quantum well dot within an infinite potential barrier. *Indian J. Pure Appl. Phys.*, 42, 908–911.
42. Wang, Q. et al. (2019). Metal-assisted photochemical etching of GaN nanowires: The role of metal distribution. *Electrochem. Commun.*, 103, 66–71. <https://doi.org/10.1016/j.elecom.2019.05.005>
43. Shaban, Z. et al. (2023). InGaN/AlInN interface with enhanced holes to improve photoelectrochemical etching and GaN device release. *Semicond. Sci. Technol.*, 38(5), 55015. <https://doi.org/10.1088/1361-6641/acc681>
44. Yu, R. et al. (2019). From bulk to porous GaN crystal: Precise structural control and its application in ultraviolet photodetectors. *J. Mater. Chem. C*, 7(45), 14116–14122. <https://doi.org/10.1039/c9tc04820k>
45. Ramesh, C. et al. (2019). Laser molecular beam epitaxy growth of porous GaN nanocolumn and nanowall network on sapphire (0001) for high responsivity ultraviolet photodetectors. *J. Alloys Comp.*, 770, 572–581. <https://doi.org/10.1016/j.jallcom.2018.08.149>
46. Shiu, G. Y. et al. (2016). InGaN light-emitting diodes with an embedded nanoporous GaN distributed Bragg reflector. *Sci. Reports*, 6, 29138. <https://doi.org/10.1038/srep29138>